Characterization of Nitronic-40 Stainless Steel Shells

Ke Han, Robert Goddard, Rongmei Niu, Yan Xin, and Vince Toplosky

***Abstract*—The construction of magnets with ever higher magnetic fields requires ever stronger and tougher reinforcement materials. Nitronic stainless steels are sometimes used for this purpose. Avoiding the sensitization temperature of these steels during fabrication is of critical importance because excessive exposure to this temperature may make them sensitive to corrosion. Even though these steels have exceptionally high mechanical strength and satisfactory toughness for use at room temperatures, low cryogenic temperatures may reduce their toughness to the degree that they are rendered unsatisfactory as reinforcement materials. This low toughness at cryogenic temperature in Nitronic steels often stems from the microstructure established during fabrication, even when the heat treatment profile follows the required protocol. Even materials that have not previously been exposed to sensitization temperatures during fabrication may later be exposed during the construction of magnets. Consequently, quality control of reinforcement materials must include both toughness tests and microstructure analyses. This paper reports recent studies of the effect of component volume and microstructure on cryogenic temperature toughness in Nitronic-type stainless steels. By comparing four different shells, we established that the presence of grain boundary particles caused lower impact fracture energy but had no significant impact on mechanical strength.**

***Index Terms*—High strength steels, alloy, deformation, high field magnet, reinforcement.**

I. Introduction

HIGH strength stainless steel is widely used as reinforcement for coils in high field magnet systems[1]–[6]. During fabrication, the material may be exposed to temperatures up to 973 °K (700 °C) for a relatively long time [7]–[9]. For example, heat treatment for up to 100 hours is required for cable-in-conduit coils with low temperature superconductors [4], [6], [10]–[14]. Under these conditions, the sensitization of stainless steel may result in a deterioration of certain mechanical properties [15]–[17]. This deterioration, such as the reduced cryogenic fracture toughness and increased crack growth rates, could be attributed to the formation of intermetallic compounds, including σ phase [18]. Alternatively, it could be attributed to grain boundary precipitates like (Fe, M1, M2, …)$_{23}$C$_6$, where M1, M2, … are alloying elements for enhancement of corrosion resistance [18]. More recent work showed that the grain boundary precipitates could instead be (Fe,Cr,Ni,Si)$_2$Mo$_{1-x}$ or (Cr, Fe)$_2$N [15], [16], [19]. Sensitization can be minimized by solution annealing at elevated temperatures, which are above 1100 °K[20]–[22]. If annealing occurs after the material has reached its final geometry, it could distort the final product, making it useless for application in a magnet[13], [14], [23]. Once a magnet is fully constructed, further annealing is impossible because it may damage other components of the magnet. Hence, characterization of materials must be done, and essential corrections must be made, before final processing [24], [25].

In this paper, we discuss which microstructure features determine cryogenic mechanical strength and toughness in Nitronic-40 stainless steels, and we include a brief discussion how to control these properties in magnet reinforcement shells.

II. Methods

A. Material Fabrication

Four Nitronic-40 cylindrical reinforcement shells were prepared by hot forging at Scott Forge (Spring Grove, Il) according to ASTM A437-17 modified according to ESA-TS-0-001. These shells were intended for use as reinforcements in the 100 T pulsed magnet. Table I gives the composition of the steels used in this work (Note: throughout this article, all compositions are quoted in weight percent. Composition in Table I was measured by Element Materials Technology, a materials characterization company.) Wall thickness of the shells varied from 79 to 116 mm (Table II). Shell inner diameters varied from 0.259 to 0.643 meter and shell height varied from 0.641 to 0.946 meter.

B. Property Characterization

Most mechanical tests were performed at 295 K and 77 K, per ASTM E8-00b and ASTM A370-97a. In tensile tests, the samples were loaded in displacement control mode. From the measured stress-strain curves, both ultimate tensile strength (TS) and 0.2% offset engineering flow stress (YS = Yield Strength) were recorded. Charpy V-notch (CVN) tests were performed per ASTM E23-00 and ASTM A37-97a. The impact energy values were recorded in Joule. These tests were used to estimate the toughness of our material [26].

Manuscript received November 28, 2020; revised March 18, 2021 and March 28, 2021; accepted March 30, 2021. Date of publication April 2, 2021; date of current version June 11, 2021. This work was completed in part in the National High Magnetic Field Laboratory, which is supported by NSF DMR-1157490 plus DMR-1644779 and in part by the State of Florida. The microscopes were funded by Florida State University Research Foundation and Florida State. *(Corresponding author: Ke Han.)*

The authors are with National High Magnetic Field Laboratory, Tallahassee, FL 32310 USA (e-mail: han@magnet.fsu.edu; goddard@magnet.fsu.edu; rniu@magnet.fsu.edu; xin@magnet.fsu.edu; toplosky@magnet.fsu.edu).

Color versions of one or more figures in this article are available at https://doi.org/10.1109/TASC.2021.3070819.

Digital Object Identifier 10.1109/TASC.2021.3070819

TABLE I
CHEMISTRY OF THE ALLOY

Elements	Mn	Ni	Cr	Mo	Si	Cu	Al	V	Nb	C	P	S	N	Sn	Ti	W	Pb	Fe
Composition (wt%)	8.82	6.92	20.27	0.28	0.72	0.38	0.02	0.05	0.02	0.03	0.023	0.001	0.362	0.01	<0.01	0.02	<0.001	Balance

TABLE II
TENSILE MECHANICAL TESTING DATA AT TWO TEMPERATURES

Shell No	Thickness (mm)	UTS (MPa) (RT)	UTS (MPa) (77 °K)	YS (MPa) (RT)	YS (MPa) (77 °K)	%El (RT)	%El (77 °K)	%RA (RT)	%RA (77 °K)
1	79	731	1530	386	1041	63	43	80	36
2	83	744	1563	396	1039	51	39	77	38
3-o	116	718	1549	405	1015	55	37	79	29
4	108	702	1509	412	984	55	41	80	34

TS = ultimate Tensile Strength, YS =flow stress at 0.2% offset, %El=Elongation to failure, and %RA = Reduction in Area at fracture.

C. Microstructure Examination

Microstructure was investigated using Zeiss 1540XB and FEI Helios G4 UC field emission gun scanning electron microscopes (FEG SEM). Energy Dispersion X-ray (EDX) spectrometers were attached to both SEMs. We also used other microscopy methods to assist our characterizations [10], [11]. The chemistry of the alloy was determined according to ASTM 751-96 and A484-16.

III. RESULTS

A. Heat Treatment on σ Phase

Nitronic-40, like most austenitic stainless steels, contains Cr, which may form σ phase under certain heat treatment conditions (Fig. 1). In the fabrication of large-volume magnet components, such as reinforcement shells, the relatively large thermal mass may lead to insufficient cooling, which can contribute to the formation of σ and other undesirable phases [17]. Our previous work indicates that, in addition to undesirable phases like σ, insufficient cooling may also generate nitride and other problematic grain boundary intermetallic compounds. These can produce lower toughness at the cryogenic temperatures at which most magnets operate.

B. Tensile Mechanical Properties

Tensile tests at room temperature, as shown in Table II, gave ultimate Tensile Strength (TS) measurements above 700 MPa, within the specification for Nitronic 40. Yield Strength (YS) values were above 350 MPa, with the maximum value at 412 MPa.

To estimate the ability of the shells to withstand plastic loading, we calculated the ratio between TS and YS (TS/YS), which yielded values above 1.5 for all components, indicating that a high rate of work-hardening occurred during testing. If further fabrication related to deformation is required for a component, we expect that it will rapidly become stronger during deformation [4], [6], [27]–[29].

We found that the values of TS/YS strain were highest in components with the smallest volume. Our curve of room

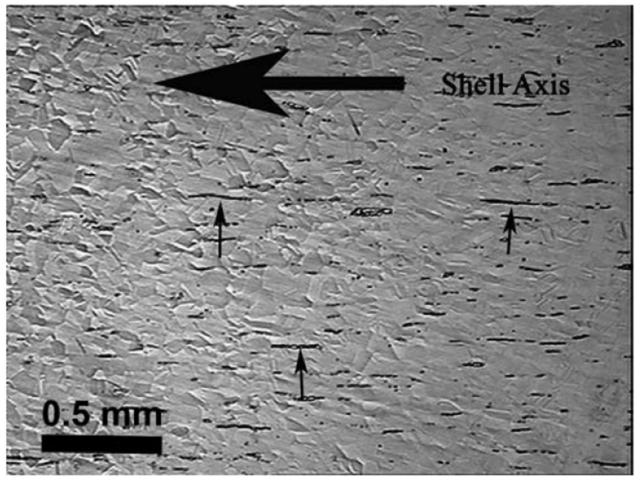

(a)

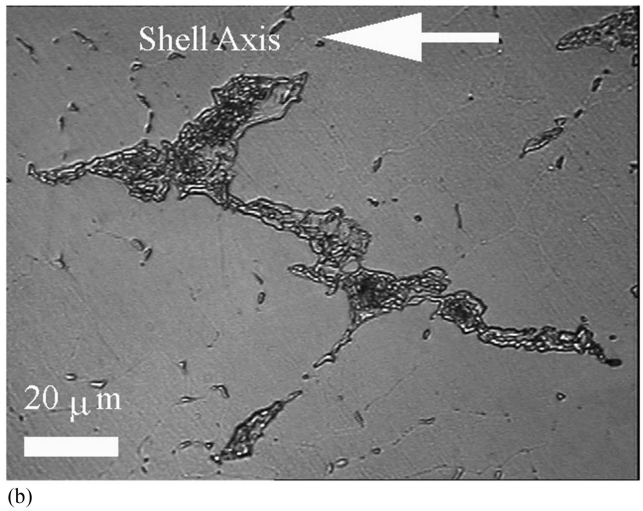

(b)

Fig. 1. Light microscopy images showing σ and ferrite phases formed in Nitronic-40. (a) Light micrograph showing dark lines of elongated ferrite formed during forging. For clarity, a few of these are indicated by small arrows. (b) Large magnification image showing several composites, each consisting of several σ phase particles inside a single ferrite grain. In the large one, two phases are separated by dark lines. In the smaller ones, dark lines are only visible in certain regions. The presence of σ phase may cause premature failure of the reinforcement at 77 °K.

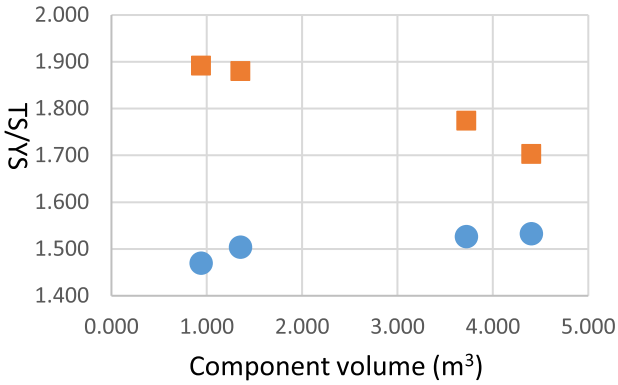

Fig. 2. Ratio of yield strength (YS) over tensile strength (TS) for four different shells with different volumes (horizontal axis). The ratio is presented as TS/YS in vertical axis. YS and TS were tested at both room temperature (solid square) and 77 K (solid circle). From left to right, data is shown from Shells 1, 2, 3-o, and 4 (thickness of 79, 83, 116, and 108 mm, respectively).

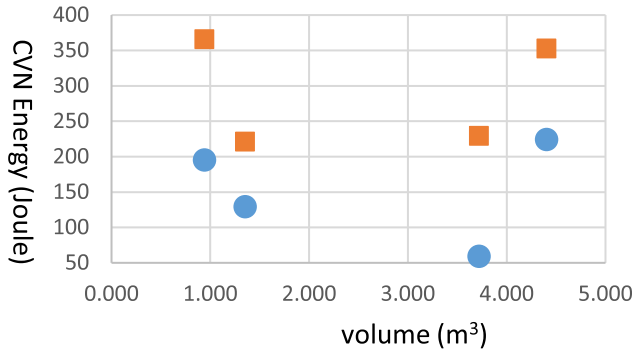

Fig. 3. Charpy V-notch data for four shells of different volume (horizontal axis). From left to right, data is shown from Shells 1, 2, 3-o, and 4 (thickness of 79, 83, 116, and 108 mm, respectively). The tests were undertaken at either 228 K (solid square) or 77 K (solid circle).

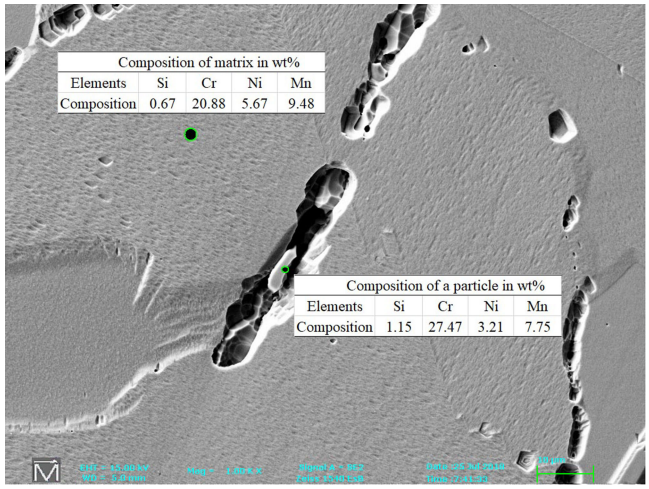

Fig. 4 Scanning electron microscopy image and EDS data showing grain boundary precipitates in Shell 3-o. Energy dispersion spectroscopy was used to detect the chemistry in the matrix (indicated by a large circle) and in the precipitate (indicated by a small circle).

temperature TS/YS values for various components of different sizes demonstrated that TS/YS decreased with volume (Fig. 2).

Values for elongation-to-failure (%El) were all above 50%, and values for reduction-in-area-at-fracture (%RA) were all above 70%. These values indicate good room-temperature ductility.

The component with the least wall thickness had the lowest YS but the highest %El. Because lower yield strength and higher elongation-to-failure can indicate lower dislocation density, we speculate that the component with the least wall thickness also had the lowest dislocation density [30]–[34].

Tensile tests of all samples at 77 °K gave TS values above 1500 MPa, about twice the corresponding room temperature values (Table II). The YS values were even greater than twice those of corresponding room temperature values. The great difference between TS and YS indicates that work-hardening occurred after materials were subjected to plastic deformation [29].

We estimated the work-hardening rate using a ratio of TS/YS. Values for all components were lower (indicating lower work-hardening rate after deformation) at 77 °K than at room temperature. Moreover, at 77 °K, the smaller the component, the lower the TS/YS values. This is the reverse of the test results at room temperature (Fig. 2).

C. CVN Data

CVN data tested at 228 °K and at 77 °K showed that three of the four shells tested (1, 2, and 4) required energy greater than 100 Joule to fracture. Shell 3-o, however, failed at less than 100 Joule at 77 K (Fig. 3). This shell had lower CVN value than the others, which we feared would lead to premature failure. We therefore replaced the original shell (Shell 3-o) with a remanufactured version (Shell 3-r).

D. Microstructure

We focused our microstructure examination on Shell 3-o because it showed lower %RA and CVN energy at 77 K. We also used Shell 4 as a comparison. Under the same etching conditions, we observed distinct grain boundaries accompanied by pitting in Shell 3-o, but we saw hardly any grain boundaries at all in Shell 4. This indicates that Shell 3-o was more susceptible to grain boundary etching. In Shell 3-o, we also observed grain boundary precipitates in the pitted regions. These precipitates were rich in Cr and poor in Ni, indicating they may have been Cr-containing intermetallics (Fig. 4).

E. Properties of Improved Component

Our newly remanufactured Shell 3-o (Shell 3-r) had tensile mechanical properties similar to those of the other shells. The CVN energy at 77 K for this new shell was above 100 J, and close examination of the shell revealed no large grain boundary precipitates.

IV. Discussion

The volume (i.e., thermal mass) of the components was large enough to affect heat treatment profiles, given the thickness of shell walls. The trend line of TS/YS at room temperature

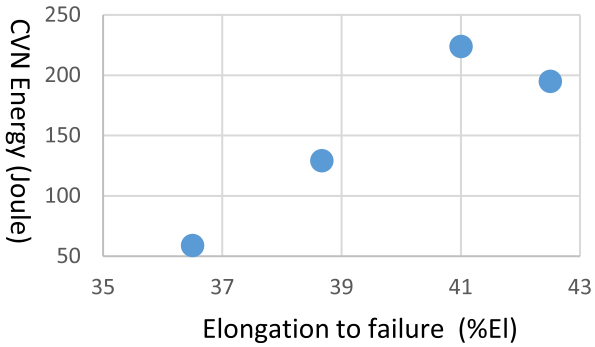

Fig. 5. Relationship between CNV and %El of shells tested at 77 °K. From left to right, data is shown from Shells 3, 2, 4, and 1 (thickness of 116, 83, 108, and 79 mm, respectively).

indicated that the smaller the thermal mass, the higher the ratio. A high ratio indicated that the materials had a greater tendency to work-hardening and thus needed higher flow stress for deformation [29]. This ratio may also affect fatigue properties of stainless steels for magnets [35]–[37].

Flow shear stress (τ) in any given metallic material can be related to dislocation densities:

$$\tau = \alpha \mu \mathrm{b}\, \delta^{0.5} \tag{1}$$

where α is a constant, μ is shear modulus, b is the Burgers vector, and δ is dislocation density. We believe that a difference in the thermal mass of a component does not change the values of α, μ, *or b.* Consequently, the value for δ will be different in different components.

The higher the thermal mass, the longer the time required for the component to reach the homogeneous temperature necessary for achieving the designated δ, provided the power of the heat treatment equipment remains the same throughout the fabrication of all shells, as was the case in our study. The component with the largest thermal mass would show the highest flow stress and/or yield strength, given the same duration of heat treatment. In other words, the higher the thermal mass, the higher the yield strength. This relationship indicated that the δ value was highest in shell 4, which had the largest thermal mass, and lowest in shell 1, which had the lowest thermal mass (Table II).

The δ value may affect both the strength and the ductility of a material, but this was not the case in our alloys. Upon examination of our room temperature data, we observed no systematic trend. All the shells showed good ductility in that the values for reduction-in-area-at-fracture did not vary significantly. At 77 °K, however, we observed lower ductility and greater variation. Shell 3-o, which had later been replaced by Shell 3-r (see result session above), showed the lowest elongation and reduction-in-area-at-fracture, and its CVN value was also the lowest (Fig. 5). This low CVN value was not related to the δ value, but rather to the grain boundary phase formed during thermal processing of the shell. The formation of the grain boundary phase may be related to the fact that Shell 3-o had the largest wall thickness. The greater the thickness, the longer the time required to reach the same heat treatment temperature. It is likely that a portion of Shell 3-o stayed at sensitization temperature sufficiently long to form undesirable grain boundary particles. Grain boundary particles may induce embrittlement in some alloys [20], [21], [38]–[40].

We used the following equation to estimate the fracture toughness ($\mathrm{K_{IC}}$) of stainless steels:

$$\mathrm{K}_{IC}{}^2/\mathrm{E} = \mathrm{C} * \mathrm{CVN} * \%\mathrm{RA} \tag{2}$$

where C is a constant between 0.8 and 0.9, E is Young's modulus (200 GPa), CVN is the Charpy V-notch value, and %RA is the percent of reduction-in-area at fracture [35], [36]. Using data taken from tensile and CVN tests, we estimated that for Shells 1, 2, 3-r, and 4, $\mathrm{K_{IC}}$ values were between 80 and 100 MPa$*$m$^{0.5}$. These values indicated that these shells had sufficient toughness for our applications, but not shell 3-o [17].

V. Conclusion

The characterization of samples from four Nitronic-40 magnet shell components of different sizes indicated that the values of TS/YS in general were lower at 77 K than at room temperature. At room temperature, the largest shell had the lowest work-hardening rate, but that rate was still higher than any of the rates at 77 K. At 77 K, on the other hand, the largest shell had the highest work-hardening rate, but it was still lower than any of the shells at room temperature. Higher thermal mass led to lower TS/YS at room temperature but higher TS/YS at 77 K.

Grain boundary precipitation had no direct impact on tensile strength or room temperature ductility, but at 77 K this kind of precipitation did lead to lower CVN test data, lower elongation, and lower reduction-in-area-at-fracture.

Acknowledgment

The authors would like to thank Scott Forge for manufacturing the component and performed some of the tests. They would also like to thank D. Nguyen for providing data concerning magnet design and to M. Tyler for editing.

References

[1] J. Bacon *et al.*, "First 100 T non-destructive magnet outer coil set," *IEEE Trans. Appl. Supercond.*, vol. 10, no. 1, pp. 514–517, 2000.
[2] M. R. Vaghar, L. Li, Y. Eyssa, H. J. Schneider-Muntau, and R. Kratz, "Roads to 100 t pulsed magnets," *IEEE Tran. Appl. Supercond.*, vol. 10, no. 1, pp. 507–509, 2000.
[3] F. Lecouturier *et al.*, "Copper/stainless steel polyhelix magnets," *IEEE Trans. Appl. Supercond.*, vol. 22, no. 3, pp. 404–404, 2012.
[4] K. Han, J. R. Sims, C. A. Swanson, and H. J. Schneider-Muntau, "Reinforcement materials for high field magnets," *IEEE Trans. Appl. Supercond.*, vol. 14, no. 2, pp. 1141–1144, 2004.
[5] L. Li *et al.*, "High performance pulsed magnets with high strength conductors and high modulus internal reinforcement," *IEEE Trans. Appl. Supercond.*, vol. 10, no. 1, pp. 542–545, 2000.
[6] K. Han *et al.*, "Material issues in the 100 T non-destructive magnet," *IEEE Trans. Appl. Supercond.*, vol. 10, no. 1, pp. 1277–1280, 2000.
[7] S. Sgobba *et al.*, "Assessment of residual stresses in ITER CS helium inlet welds fatigue tested at cryogenic temperature," *'27th Int. Cryogenics Eng. Conf. Int. Cryogenic Mater. Conf. 2018'*, Bradshaw, T., Kirichek, O., and Vandore, J. Eds. 2019.
[8] P. Libeyre *et al.*, "Manufacture of the ITER central solenoid components," *IEEE Trans. Appl. Supercond.*, vol. 28, no. 3, Apr. 2018, Art. no. 4200805

[9] D. M. McRae, S. Balachandran, and R. P. Walsh, and Iop, "Fatigue and fracture of three austenitic stainless steels at cryogenic temperatures," in *Advances Cryogenic Engineering - Materials*, (IOP Conference Series-Materials Science and Engineering), vol. 279, 2017, Art. no. 012001.

[10] S. Askenazy, L. VanBockstal, F. Dupouy, and F. Herlach, "The performance of high-field magnets with optimized internal reinforcement," *Meas. Sci. Technol.*, vol. 7, no. 4, pp. 680–685, 1996.

[11] J. Chen, K. Han, P. N. Kahl, and W. D. Markiewicz, "Deformation behavior of Nb3Sn type superconductors," *IEEE Trans. Appl. Supercond.*, vol. 15, no. 2, pp. 3568–3571, 2005.

[12] J. Chen, K. Han, P. N. Kalu, and W. D. Markiewicz, "Dispersion strengthened Nb_3Sn wire," *IEEE Trans. Appl. Supercond.*, vol. 17, no. 2, pp. 2584–2587, 2007.

[13] J. Lu, E. S. Choi, R. Walsh, R. Goddard, K. Han, and J. R. Miller, "Characterization of Nb_3Sn superconductors for hybrid magnets," *IEEE Trans. Appl. Supercond.*, vol. 17, no. 2, pp. 2651–2654, 2007.

[14] J. Lu, K. Han, R. P. Walsh, and J. R. Miller, "I-C axial strain dependence of high current density Nb_3Sn conductors," *IEEE Trans. Appl. Supercond.*, vol. 17, no. 2, pp. 2639–2642, 2007.

[15] K. Han, Y. Xin, R. Walsh, S. Downey, and P. N. Kalu, "The effects of grain boundary precipitates on cryogenic properties of aged 316-type stainless steels," *Mater. Sci. Eng. a-Struct. Mater. Properties Microstructure Process.*, vol. 516, no. 1-2, pp. 169–179, 2009.

[16] S. Downey, P. N. Kalu, and K. Han, "The effect of heat treatment on the microstructure stability of modified 316LN stainless steel," *Mater. Sci. Eng. a-Struct. Mater. Properties Microstructure Process.*, vol. 480, no. 1-2, pp. 96–100, 2008.

[17] J. R. Sims *et al.*, "The U.S. NHMFL 60T long pulse magnet failure," *IEEE Trans. Appl. Supercond.*, vol. 12, no. 1, pp. 480–483, 2002.

[18] N. Lopez, M. Cid, M. Puiggali, I. Azkarate, and A. Pelayo, "Application of double loop electrochemical potentiodynamic reactivation test to austenitic and duplex stainless steels," *Mater. Sci. Eng. a-Struct. Mater. Properties Microstructure Process.*, vol. 229, no. 1-2, pp. 123–128, 1997.

[19] I. O. Bannykh, M. A. Sevost'yanov, and M. E. Prutskov, "Effect of heat treatment on the mechanical properties and the structure of a high-nitrogen austenitic $02Kh_{20}AG_{10}N_4MFB$ steel," *Russ. Metall.*, no. 7, pp. 613–618, 2016.

[20] S. Downey, II, P. Kalu, and K. Han, "The effect of heat treatment on the microstructure stability of modified 316LN stainless steel," *Mater. Sci. Eng.: A*, vol. 480, no. 1-2, pp. 96–100, 2008.

[21] S. Downey, II, K. H, P. N. Kalu, K. Yang, and Z. Du, "A study of submicron grain boundary precipitates in ultralow carbon 316LN steels," *Metallurgical Trans. A*, vol. 41, no. 4, pp. 881–887, 2010.

[22] S. T. Downey, N. Bembridge, P. N. Kalu, H. M. Miller, G. S. Rohrer, and K. Han, "Grain boundary plane distributions in modified 316 LN steel exposed at elevated and cryogenic temperatures," *J. Mater. Sci.*, vol. 42, no. 23, pp. 9543–9547, 2007.

[23] J. Lu, K. Han, R. P. Walsh, T. Atkins, and S. T. Bole, "Critical current longitudinal and transverse strain sensitivities of high J(C) nb(3)sn conductors," *IEEE Trans. Appl. Supercond.*, vol. 18, no. 2, pp. 1014–1017, 2008.

[24] L. T. H. Nguyen, J. S. Hwang, M. S. Kim, J. H. Kim, S. K. Kim, and J. M. Lee, "Charpy impact properties of hydrogen-exposed 316L stainless steel at ambient and cryogenic temperatures," *Metals*, vol. 9, no. 6, pp. 625–625, 2019.

[25] J. J. Xin *et al.*, "Microstructure and mechanical properties of ITER correction coil case material," *IEEE Trans. Appl. Supercond.*, vol. 30, no. 2, 2020, Art. no. 4201707

[26] H. M. Ding, Y. Z. Wu, Q. J. Lu, P. Xu, J. Y. Zheng, and L. J. Wei, "Tensile properties and impact toughness of S30408 stainless steel and its welded joints at cryogenic temperatures," *Cryogenics*, vol. 92, pp. 50–59, 2018.

[27] K. Han, V. Toplosky, N. Min, J. Lu, Y. Xin, and R. Walsh, "High modulus reinforcement alloys," *IEEE Trans. Appl. Supercond.*, vol. 28, no. 3, 2018, Art. no. 0602405

[28] K. Han *et al.*, "Selected Ni alloy considerations for superconducting magnets," *IEEE Trans. Appl. Supercond.*, vol. 23, no. 3, Jun. 2013, Art. no. 7800204

[29] K. Han, V. J. Toplosky, J. Lu, Y. Xin, and R. Walsh, "Yielding and strain-hardening of reinforcement materials," *IEEE Trans. Appl. Supercond.*, vol. 29, no. 5, Aug. 2019, Art. no. 7800405.

[30] K. Han, "Property of ultrafine grained engineering materials related to high magnetic fields," *Ultrafine Grained Mater. IV*, pp. 473–480, 2006.

[31] K. Han, "Strength and ductility of nanostructured composites with co-deformable components," in *Ductility of Bulk Nanostructured Materials*, (Materials Science Forum), vol. 633–634, Zhao,Y., and Liao,X. Eds. 2010, pp. 383–392.

[32] K. Han, and J. P. Chen, "Achievable strength of nanostructured composites with Co-deformable components," in *Advanced Mechanical Properties and Deformation Mechanisms of Bulk Nanostructured Materials*, (Materials Science Forum), vol. 683, Zhao, Y. H. Ed., 2011, pp. 243–247.

[33] J. D. Embury, "Structural aspects of materials subjected to large strains," *Mater. Sci. Eng. a-Struct. Mater. Properties Microstructure Process.*, vol. 175, no. 1-2, pp. 105–111, 1994.

[34] J. D. Embury, and K. Han, "Dislocation accumulation at large plastic strains - An approach to the theoretical strength of materials," *Prog. Mech. Behav. Mater. (Icm8)*, vol. 2, pp. 448–457, 352, 1999.

[35] K. Han, R. P. Walsh, V. J. Toplosky, R. Goddard, and M. D. Bird, "Microstructure and cryogenic mechanical properties of a 316L plate and its weldments," *Advances in Cryogenic Engineering, Vol 52a & 52b* Balachandran, U. Ed. 2006, pp. 99–106.

[36] K. Han, R. P. Walsh, V. J. Toplosky, R. E. Goddard, J. Lu, and I. R. Dixon, "Effects of winding strain and heat treatment on properties of 316 LN and haynes 242," *Advances in Cryogenic Engineering, Vol 54: Transactions of the International Cryogenic Materials Conference - Icmc* Balachandran, U.B. Ed. 2008, pp. 84–91.

[37] V. J. Toplosky, R. P. Walsh, and K. Han, "Fatigue properties of modified 316ln stainless steel at 4 k for high field cable-in-conduit applications," in *Advances in Cryogenic Engineering* Balachandran, vol. 56, U. Ed., 2010, pp. 9–16.

[38] K. Han, D. V. Edmonds, and G. D. W. Smith, "Optimization of mechanical properties of high-carbon pearlitic steels with SI and V additions," *Metallurgical Mater. Trans. a-Phys. Metall. Mater. Sci.*, vol. 32, no. 6, pp. 1313–1324, 2001.

[39] K. Han, T. D. Mottishaw, G. D. W. Smith, and D. V. Edmonds, "Effects of vanadium addition on nucleation and growth of pearlite in high-carbon steel," *Mater. Sci. Technol.*, vol. 10, no. 11, pp. 955–963, 1994.

[40] K. Han, G. D. W. Smith, and D. V. Edmonds, "Pearlite phase-transformation in SI and V steel," *Metallurgical Mater. Trans. a-Phys. Metall. Mater. Sci.*, vol. 26, no. 7, pp. 1617–1631, 1995.